The Height Of Accuracy:
Recovering Height Information from before the Leading Edge

Graham Quartly

National Oceanography Centre, UK

Introduction

Ocean altimetry processing usually assumes the reflecting surface is homogeneous, allowing a simple expression for the curve to be fitted to the waveforms. Where inhomogeneities occur, their effect will be seen to migrate through 2-D waveform space, as the range from the altimeter to a fixed point on the Earth varies as a hyperbolic function of time. Each anomalous scatterer generates the same-shaped feature; what needs to be determined is the **amplitude** of the feature, and its **position** within waveform space.

Extra path delay, relative to sea level at nadir, ξ, is given by:

$$(H + \xi)^2 = (H - h)^2 + \rho^2$$

where, distance, ρ, combines both nearest approach, x_0, and position along track, viz:

$$\rho^2 = x_0^2 + v^2 t^2$$

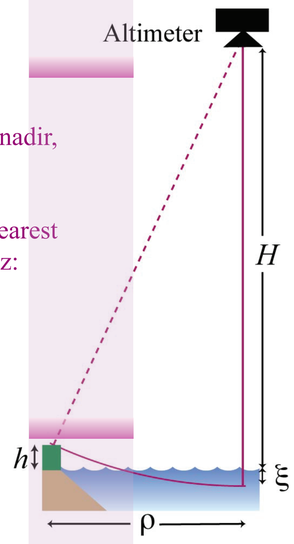

Simple hyperbola — point target

A small strong reflector above the sea surface produces a clear hyperbola, which is easily detected above the thermal noise. Tournadre (2007) showed a number of examples for reflections from ships or lighthouses. The illustration here shows returns from a number of ships near entrance to Suez Canal, showing a sharp echo even in 90 Hz waveforms (averaging of Envisat IEs in groups of 20). [A further case study of IE analysis is shown in Quartly (2010).]

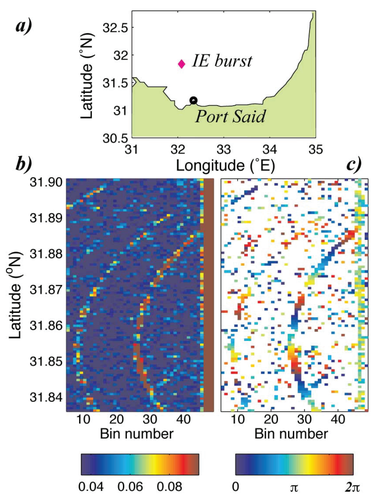

Analysis of Envisat Individual Echoes in the SE Mediterranean Sea. a) Location, b) Amplitude averaged in groups of 20 (i.e. ~90 Hz waveforms), c) Phas difference between consecutive IEs, averaged in groups of 20; phase difference only shown where phase change is internally consistent.

[Note only bins prior to leading edge are shown here.]

Envelope of hyperbolae — cluster of targets

In the case of Pianosa, there are often a number of weak reflections from the land, generating a host of hyperbolic curves within the thermal noise region. Rather than attempt to fit each individually, we can fit an envelope function to encompass the majority of them (assuming island is of small spatial extent). The fitted envelope then gives the height and location of the peak of the ridge underlying the overflight. This technique can work even where the nominal location of the apex is before the first bin of the waveform.

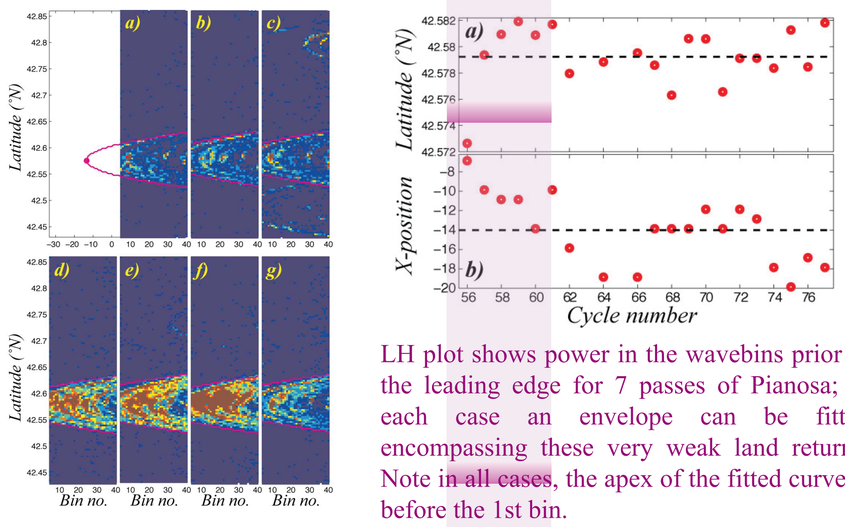

LH plot shows power in the wavebins prior to the leading edge for 7 passes of Pianosa; in each case an envelope can be fitted encompassing these very weak land returns. Note in all cases, the apex of the fitted curve is before the 1st bin.

RH plot shows statistics of fitted envelopes, giving the consistency of the results achieved.

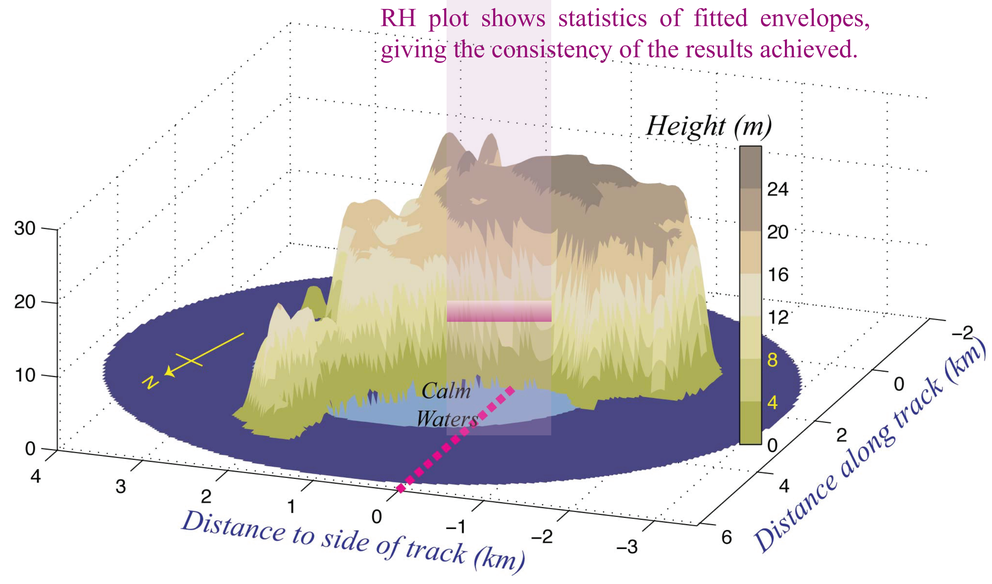

Digital Elevation Model of Pianosa, with backscatter properties of sea surface modified in northern bay.

Simulation & Retrieval

A simple summation is made of the reflections from a given part of the Earth's surface, with each pixel having its own backscatter strength, mean height and variability (akin to SWH). For most of the region, mean height is zero and backscatter is 0 dB. The features of interest may be on the nadir track or to one side, can be above sea level and have reduced or increased backscatter strength.
In a noise-free situation with a perfect simulation and a matching model, it is not difficult to recover the location of a simulated feature. Tournadre et al. (2008) have developed such a technique for automatically measuring the height of icebergs. If a collection of individual targets are close together, the algorithm must be able to estimate each in the presence of others.

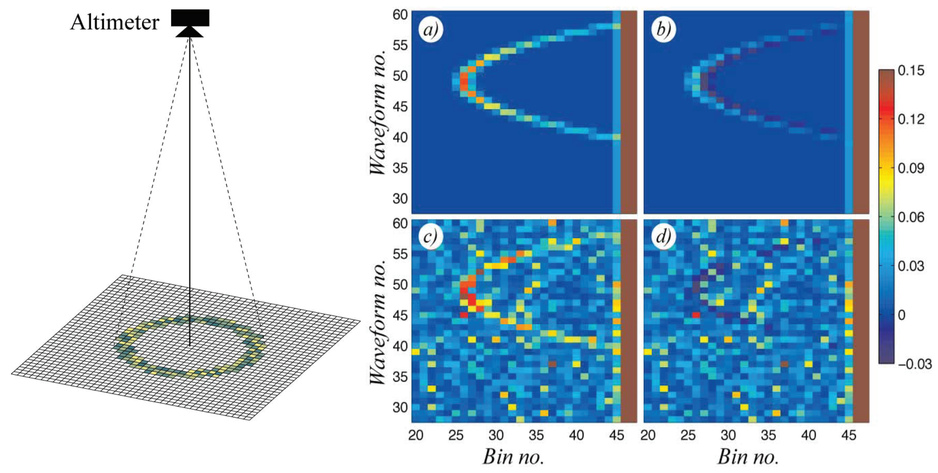

The simulation uses a narrow grid of surface pixels, characterised by height, variability in height and relative signal strength (see Quartly et al., 1999).
a) Small simulated feature ahead of leading edge (bin 45), b) Resultant after feature removed using incomplete model, c) Simulation with added noise, d) Resultant from previous simulation once feature has been estimated and removed using correct model.

Broad features — bright targets & rain

Very small features on the sea surface will not be detectable amidst the Rayleigh (fading) noise. Areas > 1km X 1km may be detectable depending upon the magnitude of the change. This work was developed through the investigation of rain (where attenuation in the atmospheric column mimics the effect of reduced surface backscatter). Tournadre (1998) demonstrated the fitting of Gaussian or cylindrically symmetrical rain rate models to the waveform data, whilst Quartly (1998) showed the estimation of backscatter/attenuation for multiple square tiles along and across track, pointing the way towards studies of backscatter variation at scales smaller than the instrument footprint.

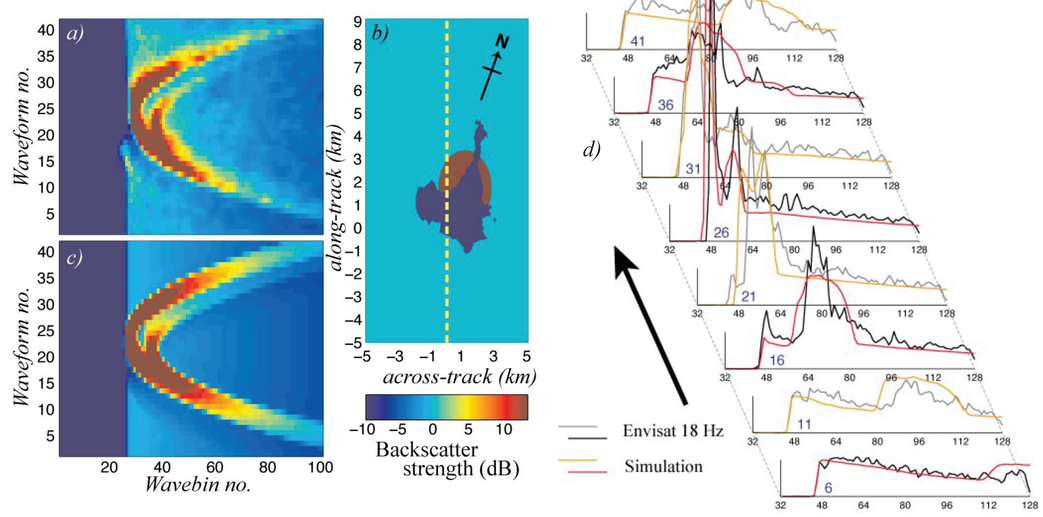

a) Envisat 18 Hz waveforms for altimeter pass over Pianosa, discssed in Gómez-Enri et al. (2010). Note the first 20 bins of thermal noise are not shown, so the leading edge is at 26, with the anomalous "bright target" hyperbolic response dominating the general ocean signal.
b) Surface scattering model of Pianosa, with y-axis along RA-2 track, and reduced scatter over island, plus a disc of increased scattering strength.
c) Resultant simulated waveforms — note the use of 2 bays in simulation to produce hyperbolae with different locations along and across-track.
d) Comparison of every 5th waveform from real and simulated datasets..

Further developments

Further work is required to optimise the simulation, and hence hone the coefficients required for the inversion. This is especially the case for hyperbolae peaking before the first wavebin. Processing of a single altimeter pass still leaves ambiguity as to whether the strongest reflecting point of an island lies on the nadir track, or whether the derived range information includes a contribution from across-track delay. Assuming the locations of the strongest reflectors remain fixed (rather than being ephemeral lakes or bogs) then processing of multiple passes within the ±1 km dead-band will help resolve this issue.

References

Gómez-Enrí, J. et al (2010), Modeling Envisat RA-2 waveforms in the coastal zone, *IEEE Geosci. Rem. Sens. Lett.* 7 (3), 474-478.
Quartly G.D. (1998), Determination of oceanic rain rate and rain cell structure from altimeter waveform data. Part I: Theory, *J. Atmos. Oceanic Tech.* 15, 1361-1378.
Quartly G.D., et al. (1999), Understanding the effects of rain on radar altimeter waveforms, *Adv. in Space Res.* 22, 1567-1570.
Quartly (2010), Hyperbolic retracker: Removing bright target artefacts from altimetric waveform data, *Proc. of ESA Living Planet Symposium*, Bergen, ESA SP-686.
Tournadre (1998), Determination of rain cell characteristics from the analysis of Topex altimeter echo waveforms, *J. Atmos. Ocean. Tech.*, 15 (2), 387–406.
Tournadre J. (2007), Signature of lighthouses, ships, and small islands in altimeter waveforms, *J. Atmos. Oceanic Tech.* 24, 1143-1149.
Tournadre J. et al (2008), Iceberg detection in open water by altimeter waveform analysis, *J. Geophys. Res*. 113, art. no. C08040.

Acknowledgements

The 18 Hz waveform data were obtained from ESA through the Cat-1 proposal ARIES (Accurate Rain Information from Envsiat Sensors) and the IEs under the project RAIES (Radar Altimeter Individual Echoes and S-band). This work has been supported by ESA through the COASTALT programme (http://www.coastalt.eu).